Polarized Specular Reflectance Spectra of Fe(β-dtpy)$_2$·4THF: A D_{2h} Model of Porphyrins

Christopher B. Hoffman,[1a] Vincenzo Fares,*[,1b] Alberto Flamini,*[,1b] and Ronald L. Musselman*[,1a]

Department of Chemistry, Franklin and Marshall College, Lancaster, Pennsylvania 17604, and Istituto di Chimica dei Materiali del CNR, Area della Ricerca di Roma, P.O. Box 10, 00016 Monterotondo St., Roma, Italy

Received August 18, 1998

Transition metal complexes of β-dtpy (1,2,6,7-tetracyano-3,5-dihydro-3,5-diiminopyrrolizinide) are spectrally similar to metallophthalocyanines (derivatives of porphyrin) but with the advantage of being D_{2h} instead of D_{4h} so that many degenerate electronic transitions are identifiable separately. We have prepared and characterized Fe(β-dtpy)$_2$·4THF, whose crystal structure allows three spectral polarizations to be measured. We have assigned the visible and ultraviolet transitions that correspond to the Q and Soret regions of porphyrinic complexes; these assignments differ markedly from the traditional "four-orbital" model. The secondary Q peak (R) is a separate electronic transition rather than a vibronic component, and the Soret transition has been reassigned.

Square-planar complexes, including transition metal porphyrinic complexes, comprise an extremely important class of compounds, being at the center of numerous proteins, enzymes, and one-dimensional conductors.[2−36] Assignments of the simplest of these complexes, such as tetracyano complexes, have been well established.[37−45] The more complex porphyrinic complexes have had an accepted assignment of the two principal regions, the Q region in the long visible and the Soret region in the near UV,[8,9] but recent calculations have suggested that a change in assignments is appropriate.[46−48] Polarized electronic spectra have been helpful in making transition assignments, and

* Authors to whom correspondence should be addressed.
(1) (a) Franklin and Marshall College. (b) Istituto di Chimica dei Materiali del CNR.
(2) Dolphin, D., Ed. *The Porphyrins, Physical Chemistry Part A;* Harcourt Brace Jovanovich: New York, 1978.
(3) Edwards, L.; Gouterman, M. *J. Mol. Spectrosc.* **1970**, *33*, 292−310.
(4) Elissa, B. D.; Hinchliffe, A. *Theochem. J. Mol. Struct.* **1981**, *2*, 69.
(5) Estiu, G. L.; Jubert, A. H.; Costamagna, J.; Vargas, J. *Inorg. Chem.* **1996**, *35*, 263−266.
(6) Ghosh, A.; Gassman, P. G.; Almlof, J. *J. Am. Chem. Soc.* **1994**, *116*, 1932−1940.
(7) Gouterman, M. *J. Mol. Spectrosc.* **1961**, *6*, 138.
(8) Gouterman, M.; Wagniere, G. H.; Snyder, L. C. *J. Mol. Spectrosc.* **1963**, *11*, 108.
(9) Gouterman, M. In *The Porphyrins;* Dolphin, D., Ed.; Academic Press: New York, 1978; pp 1−166.
(10) Gunter, M. J.; Turner, P. *Coord. Chem. Rev.* **1991**, *108*, 115−161.
(11) Isaac, M. F.; Lin, Q.; Simonis, U.; Suffian, D. J.; Wilson, D. L.; Walker, F. A. *Inorg. Chem.* **1993**, *32*, 4030−4041.
(12) Jentzen, W.; Turowskatyrk, I.; Scheidt, W. R.; Shelnutt, J. A. *Inorg. Chem.* **1996**, *35*, 3559−3567.
(13) Komatsu, T.; Nakao, K.; Nishide, H.; Tsuchida, E. *J. Chem. Soc., Chem. Commun.* **1993**, 728−730.
(14) Mack, J.; Kirkby, S.; Ough, E. A.; Stillman, M. J. *Inorg. Chem.* **1992**, *31*, 1717−1719.
(15) McHugh, A. J.; Gouterman, M.; Weiss, J. C. *Theor. Chim. Acta* **1972**, *24*, 346.
(16) Mosseri, S.; Mialocq, J. C.; Perly, B.; Hambright, P. *J. Phys. Chem.* **1991**, *95*, 4659−4663.
(17) Mullins, J. A.; Adler, A. D.; Hochstrasser, R. M. *J. Chem. Phys.* **1965**, *43*, 2548.
(18) Musselman, R. L. In *Microbeam Analysis;* Russell, P. E., Ed.; San Francisco Press: San Francisco, CA, 1989; pp 151−157.
(19) Nesset, M. J. M.; Shokhirev, N. V.; Enemark, P. D.; Jacobson, S. E.; Walker, F. A. *Inorg. Chem.* **1996**, *35*, 5188−5200.
(20) Ono, N.; Wada, H. *J. Synth. Org. Chem. Jpn.* **1993**, *51*, 826−841.
(21) Phillips, T. E.; Hoffman, B. M. *J. Am. Chem. Soc.* **1977**, *99*, 7734.
(22) Rabinowitch, E. *Rev. Mod. Phys.* **1944**, *16*, 226.
(23) Sayer, P.; Gouterman, M.; Connell, C. R. *Acc. Chem. Res.* **1982**, *15*, 73.
(24) Schaffer, A. M.; Gouterman, M. *Theor. Chim. Acta* **1972**, *25*, 62.
(25) Schaffer, A. M.; Gouterman, M.; Davidson, E. R. *Theor. Chim. Acta* **1973**, *30*, 9−30.
(26) Seely, G. R. *J. Chem. Phys.* **1957**, *27*, 125.
(27) Rush, T.; Kumble, R.; Mukherjee, A.; Blackwood, M. E.; Spiro, T. G. *J. Phys. Chem.* **1996**, *100*, 12076−12085.
(28) Reek, J. N. H.; Rowan, A. E.; de Gelder, R.; Beurskens, P. T.; Crossley, M. J.; DeFeyter, S.; de Schryver, F.; Nolte, R. J. M. *Angew. Chem., Int. Ed. Engl.* **1997**, *36*, 361−363.
(29) Senge, M. O.; Medforth, C. J.; Forsyth, T. P.; Lee, D. A.; Olmstead, M. M.; Jentzen, W.; Pandey, R. K.; Shelnutt, J. A.; Smith, K. M. *Inorg. Chem.* **1997**, *36*, 1149−1163.
(30) Soares, L. d. A.; Trsic, M.; Berno, B.; Aroca, R. *Spectrochim. Acta, Part A* **1996**, *52*, 1245−1253.
(31) Stanley, K. D.; Delavega, R. L.; Quirke, J. M. E.; Beato, B. D.; Yost, R. A. *Chem. Geol.* **1991**, *91*, 169−183.
(32) Summerville, D. A.; Jones, R. D.; Hoffman, B. M.; Basolo, F. *J. Am. Chem. Soc.* **1977**, *99*, 8195.
(33) Umezawa, Y.; Yamamura, T. *J. Chem. Soc., Chem. Commun.* **1978**, 1106.
(34) Umezawa, Y.; Yamamura, T. *J. Electroanal. Chem.* **1979**, *95*, 113.
(35) Weiss, C.; Kobayashi, H.; Gouterman, M. *J. Mol. Spectrosc.* **1965**, *16*, 415.
(36) Yamamoto, Y.; Noro, T.; Ohno, K. *Int. J. Quantum Chem.* **1992**, *42*, 1563−1575.
(37) Marsh, D. G.; Miller, J. S. *Inorg. Chem.* **1976**, *15*, 720.
(38) Cowman, C. D.; Ballhausen, C. J.; Gray, H. B. *J. Am. Chem. Soc.* **1973**, *95*, 7873.
(39) Ballhausen, C. J.; Bjerrum, N.; Dingle, R. *Inorg. Chem.* **1965**, *4*, 514.
(40) Piepho, S. B.; Schatz, P. N.; McCaffery, A. J. *J. Am. Chem. Soc.* **1969**, *91*, 5994.
(41) Tuszynski, W.; Gliemann, G. *Ber. Bunsen-Ges. Phys. Chem.* **1985**, *89*, 940.
(42) Musselman, R. L. Ph.D. Dissertation, New Mexico State University, 1971.
(43) Anex, B. G.; Musselman, R. L. *J. Phys. Chem.* **1980**, *84*, 883−887.
(44) Musselman, R. L.; Cornelius, J. B.; Trapp, R. M. *Inorg. Chem.* **1981**, *20*, 1931−1932.
(45) Musselman, R. L.; Anex, B. G. *J. Phys. Chem.* **1987**, *91*, 4460−4463.
(46) Kutzler, F. W.; Ellis, D. E. *J. Chem. Phys.* **1986**, *84*, 1033.
(47) Liang, X. L.; Ellis, D. E.; Gubanova, O. V.; Hoffman, B. M.; Musselman, R. L. *Int. J. Quantum Chem.* **1994**, *52*, 657−671.
(48) Liang, X.; Flores, S.; Ellis, D. E.; Hoffman, B. M.; Musselman, R. L. *J. Chem. Phys.* **1991**, *95*, 403−417.

10.1021/ic980990d CCC: $18.00 © 1999 American Chemical Society
Published on Web 11/19/1999

we have proposed a new set of assignments for metallophthalocyanines (Mpc, where pc = tetraazatetrabenzoporphyrin) using a reduced-symmetry complex and results from earlier SCF-Xα-DOS calculations.[49−52]

A disadvantage of the D_{4h} symmetry of porphrinic systems is the degeneracy of many orbitals and the in-plane transitions involving these. We recently reported on a zinc complex, Zn(β-dtpy)$_2$·4THF, where dtpy = 1,2,6,7-tetracyano-3,5-dihydro-3,5-diiminopyrrolizinde,[53] which has a spectrum very similar to that of the phthalocyanines but has the advantage of D_{2h} symmetry with no orbital degeneracies. The morphology of the crystals, however, did not allow for complete separation of the three polarizations. We have now prepared Fe(β-dtpy)$_2$·4THF (FeL_2·4THF), also having D_{2h} symmetry, in which the morphology provides a distinct separation of polarizations, and we report on the results here. The experimental results have allowed a clear delineation between the two principal theoretical interpretations of porphyrinic complexes.

Experimental Section

Single-Crystal Polarized Reflectance Spectroscopy. Polarized specular reflectance spectra were obtained with a new instrument which is a major upgrade of our previous reflectance instrument.[54] The current instrument is a single beam, wide range, fast spectrophotometer. Light sources are a xenon arc lamp and a tungsten−halogen lamp, the polarizer is a MgF_2 Rochon prism, and optics are spherical and planar reflectors with an Ealing Optics reflecting objective. The image beam size is 30 μm, sample and reference mirror motions are computer controlled, UV and visible dispersion is through an Acton Research SpectraPro 275 spectrograph, and detection is with a Princeton Instruments 1152 × 296 EEV (English Electric Valve) CCD (charge-coupled device), maintained at 110 K. Spectra were recorded from the $(00\bar{1})$ and $(\bar{1}10)$ faces of a single crystal of FeL_2·4THF. The average of 50 spectra is reported in each case; the exposure time for each ranged from 0.01 to 20 s, depending on the spectral region. The data were corrected for percent reflectivity relative to an NIST standard mirror. For Kramers−Kronig analysis,[55,56] reflectivities beyond our experimental region were estimated in the infrared region from values for Ni(pc)I and Co(pc)I[57,58] and were approximated in the vacuum ultraviolet and beyond so as to produce baselines approaching zero absorbance in regions having no absorbance in solution spectra. Deconvolution was carried out with an interactive Gaussian and Lorentzian program ("FastGauss"[59]) on a Macintosh computer.

Magnetic Measurements. The magnetic measurements were carried out by using the Gouy method at room temperature. Molar susceptibility was corrected for intrinsic diamagnetism estimated from Pascal's constants.

Materials. Solvents were dried and freshly distilled under dinitrogen before use. LH was made by following our procedure already given.[60] Anhydrous $FeCl_3$ was prepared from commercial $FeCl_3$·$6H_2O$ (Fluka) as descibed in the literature.[61] The corresponding THF adduct, $FeCl_3$·*x*THF, was isolated as yellow-brown powder by extracting $FeCl_3$ in a Soxhlet apparatus under dinitrogen.

Synthesis and Properties of FeL_2·4THF. LH (0.2 g, 0.86 mmol) was added to a THF solution (100 mL) of $FeCl_3$·*x*THF (1.0 g) at room temperature under N_2. Evaporation of the resulting intense blue solution to about half of the initial volume produced FeL_2·4THF, which was isolated as golden microcrystals after filtration, washed with THF, and dried under a stream of N_2 (0.22 g, 60%). IR and X-ray powder diffraction data were coincident with those already given for the same complex prepared by following a different procedure.[62] In the solid state FeL_2·4THF is air-stable except for loss of THF by drying or through substitution by water. Therefore, the crystals must be stored in the presence of their mother liquor. Elemental analytical data were not reproducible due to partial loss of THF, even when in an H_2O-free environment. FeL_2·4THF is soluble in acetone, ethanol, methanol, and MeCN and insoluble in THF. In solution it is oxygen sensitive. Its stability in solution with respect to ligand substitution by the solvent follows the order acetone > alcohols ≫ MeCN, provided that the solvent is thoroughly dried, since water displaces L from Fe(II) very readily. FeL_2·4THF is a high-spin complex like the analogous FeL_2·2DME complex (DME = 1,2-dimethoxyethane).[62]

Crystal Growth of FeL_2·4THF. Suitable crystals for both X-ray diffraction and spectroscopic studies were grown as follows. A hot saturated solution of the compounds in a THF−MeCN (1:1) mixture was filtered and sealed in a vial under vacuum; on very slow cooling from 85 °C to room temperature over 4 days plateletlike crystals separated. Several attempts to grow large crystals of FeL_2·4THF failed; only plateletlike, low-diffracting small crystals were available. Since they are unstable in air, a single crystal was selected and sealed in a glass capillary in the presence of mother liquor.

X-ray Structure Determination. Oscillation and Weissenberg long-exposed photographs allowed selection of the space group *C*2/*c* on the basis of the systematic absences. Precise cell parameters were determined by least-squares fit of 15 well-centered medium-angle reflections. Data were collected using the $\theta-2\theta$ scan technique in the range $3° \le 2\theta \le 50°$ on a Nicolet $P2_1$ four-circle diffractometer with graphite-monochromated Mo Kα radiation (λ = 0.710 73 Å). Two check reflections measured after every 100 reflections showed no intensity reduction. Data were corrected for Lorentz−polarization effects, and a semiempirical absorption correction was done, on the basis of an azimuthal scan of three reflections. Although 8255 possible reflections were accurately measured, only a small set of 935 data had statistically significant intensities and were collected. Of these, 709 independent reflections for which $I > 2\sigma(I)$ were used throughout the calculations.

The structure was easily solved by conventional Patterson and Fourier methods. Given the small number of observations, the non-hydrogen atoms were refined only isotropically by full-matrix least-squares procedures; hydrogens were added at calculated positions with fixed U = 0.08 Å. Calculations were made by using the SHELXTL set of programs.[63] Crystal data and some experimental details are given in Table 1.

Results

Description of the Structure. The molecular structure of the title compound is shown in Figure 1: it closely resembles that of the homologous zinc complex Zn(β-dtpy)$_2$·4THF already reported.[53] In both cases the metal atom is surrounded by four imino nitrogens from two β-dtpy ligands and by two THF oxygen atoms in a tetragonally elongated octahedral geometry,

(49) Murata, K.; Liou, K.; Thompson, J.; McGhee, E. M.; Rende, D. E.; Musselman, R. L.; Hoffman, B. M.; Ibers, J. A. *Inorg. Chem.* **1997**, *33*, 3363.
(50) Liou, K. Y.; Newcomb, T. P.; Heagy, M. D.; Thompson, J. A.; Heuer, W. B.; Musselman, R. L.; Jacobsen, C. S.; Hoffman, B. M.; Ibers, J. A. *Inorg. Chem.* **1992**, *31*, 4517−4523.
(51) Rende, D. E.; Heagy, M. D.; Heuer, W. M.; Liou, K.; Thompson, J. A.; Hoffman, B. M.; Musselman, R. L. *Inorg. Chem.* **1992**, *31*, 352−358.
(52) Heagy, M. D.; Rende, D. E.; Shaffer, G. W.; Wolfe, B. M.; Liou, K.; Hoffman, B. M.; Musselman, R. L. *Inorg. Chem.* **1989**, *28*, 283−286.
(53) Fares, V.; Flamini, A.; Jasin, J. R.; Musselman, R. L.; Poli, N. *J. Chem. Soc., Dalton Trans.* **1995**, 281−286.
(54) Desjardins, S. R.; Penfield, K. W.; Cohen, S. L.; Musselman, R. L.; Solomon, E. I. *J. Am. Chem. Soc.* **1983**, *105*, 4590−4603.
(55) Anex, B. G. *Mol. Cryst.* **1966**, *1*, 1−36.
(56) Kronig, R. *J. Opt. Soc. Am.* **1926**, *12*, 547−557.
(57) Martinsen, J.; Palmer, S. M.; Tanaka, J.; Greene, R. C.; Hoffman, B. M. *Phys. Rev. B* **1984**, *30*, 6269−6276.
(58) Martinsen, J.; Stanton, J. L.; Greene, R. L.; Tanaka, J.; Hoffman, B. M.; Ibers, J. A. *J. Am. Chem. Soc.* **1985**, *107*, 6915−6920.
(59) Haddon, H.; Musselman, R. L. FastGauss, Franklin and Marshall College.
(60) Fares, V.; Flamini, A.; Poli, N. *J. Am. Chem. Soc.* **1995**, *117*, 11580.
(61) Pray, A. R. *Inorg. Synth.* **1957**, *5*, 153.
(62) Bonamico, M.; Fares, V.; Flamini, A.; Poli, N. *J. Chem. Soc., Dalton Trans.* **1992**, 3273−3280.
(63) SHELXTL PC Siemens Crystallographic Research System, Siemens Analytical X-ray Instruments Inc., Madison, WI.

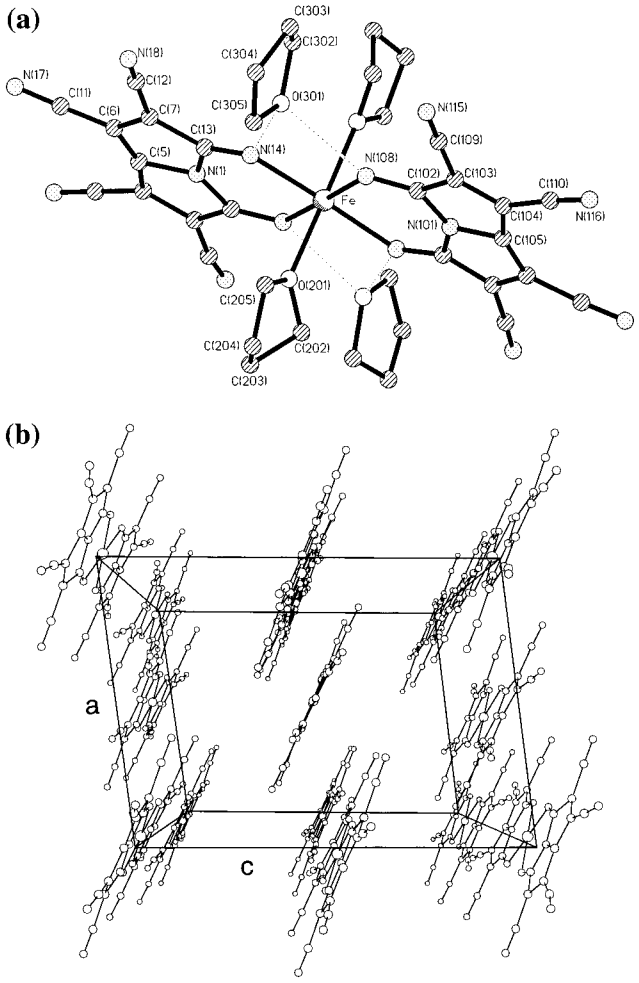

Figure 1. (a) Perspective drawing and labeling scheme of $FeL_2 \cdot 4THF$. (b) Packing diagram, with THF molecules omitted.

Table 1. Crystal Data

chem formula	$C_{38}H_{36}FeN_{14}O_4$
cryst system	monoclinic
space group	*C*2/*c*
unit cell dimens	$a = 12.388(3)$ Å
	$b = 20.237(5)$ Å
	$c = 17.067(4)$ Å
	$\beta = 97.98(2)°$
V	4237(2) Å^3
Z	4
fw	808.7
density (calcd)	1.268 Mg/m^3
abs coeff	0.411 mm^{-1}
temp (K)	293
final *R* indices (obsd data)	R = 9.76%, wR = 13.79%

while other two THF molecules are equatorially linked to the imino hydrogens. In this case, however, the planar FeL_2 complex unit has its molecular *x* axis C(5)−N(1)−Fe−N(101)−C(105) parallel to the crystallographic *y* direction and coincident with the crystallographic 2-fold axis [0, *y*, $^1/_4$], so that the two longitudinal halves of the complex are symmetrically equivalent, the molecular rms plane forming an angle of ca. 32° with the $(00\bar{1})$ plane and 69° with the crystallographic *z* direction (Figure 2).

The Fe−N_{eq} distances of 2.10 Å (mean value) and Fe−O_{ax} of 2.22 Å are consistent with a six-coordinated iron(II) in a high-spin electronic configuration, as widely discussed previously.[62] In Table 2 selected intramolecular distances and angles are reported: they are comparable with those found in the other analogous $M^{II}(\beta\text{-dtpy})_2$ complexes (M^{II} = Fe, Co, Ni, Cu, Zn, Pd) already characterized.[53,62,64−66] The presence of two independent THF solvent molecules, with an intrinsically disordered twist/envelope ring conformation,[67,68] and a high degree of mosaic spread observed in the examined crystals strongly affect the number and quality of the experimental data and, consequently, the accuracy of the geometrical results, as evidenced by large esd's and high atomic thermal parameters.

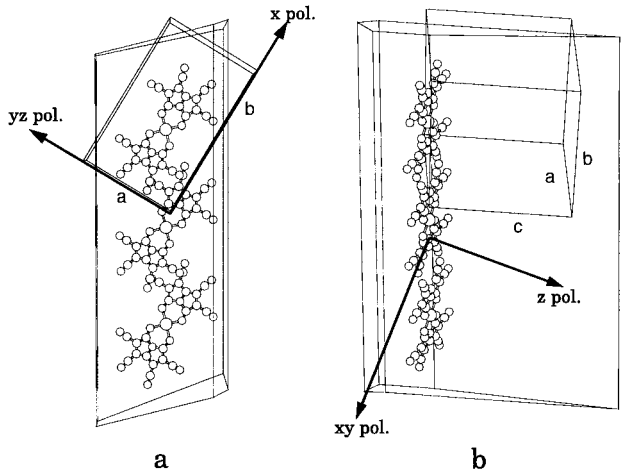

Figure 2. View of three molecules enclosed in a scaled-down representation of the crystal morphology, viewed normal to (a) the $(00\bar{1})$ face and (b) the $(\bar{1}10)$ face. The THF molecules have been omitted for clarity.

Table 2. Selected Average Bond Lengths (Å) and Angles (deg)

Fe−N (eq)	2.105(9)	Fe−O (ax)	2.223(7)
N(1)−C(5)	1.41(2)	N(1)−C(13)	1.37(1)
C(5)−C(6)	1.36(1)	C(6)−C(7)	1.38(2)
C(6)−C(11)	1.44(2)	C(7)−C(12)	1.46(2)
C(7)−C(13)	1.45(2)	C(11)−N(17)	1.13(2)
C(12)−N(18)	1.12(2)	C(13)−N(14)	1.29(2)
N(14)−Fe−N(108)	88.7(3)	N(14)−Fe−O(201)	90.2(3)
N(108)−Fe−O(201)	91.9(3)	N(14)−Fe−N(14′)	91.7(5)
N(108)−Fe−N(14′)	178.8(4)	O(201)−Fe−N(14′)	89.3(3)
N(14)−Fe−N(108′)	178.8(4)	N(108)−Fe−N(108′)	91.0(5)
O(201)−Fe−N(108′)	88.6(3)	N(14)−Fe−O(201′)	89.3(3)
N(108)−Fe−O(201′)	88.6(3)	O(201)−Fe−O(201′)	179.3(4)

The face identities were determined through single-crystal film X-ray photos[69]and interfacial angle calculations.[70]

A projection program using Mathematica on a Macintosh computer allowed determination of the magnitudes and angles of the projections of molecular vectors onto all natural crystal faces. The *x* vector is the long in-plane axis, *y* is the short in-plane axis, and *z* is normal to the plane. The most suitable faces for separating these directions spectroscopically were the $(00\bar{1})$ and $(\bar{1}10)$ faces. Views normal to both faces are shown for a typical crystal with the morphology superimposed on the crystal structure in Figure 2a,b. A unit cell is included on each drawing. The *x*, *y*, and *z* contributions to each polarization of the spectra are given in Table 3, calculated using $I = (\cos(q)|\mathbf{v}|)^2$, where **v**

(64) Bonamico, M.; Fares, V.; Flamini, A.; Poli, N. *Inorg. Chem.* **1991**, *30*, 3081−3087.
(65) Bonamico, M.; Fares, V.; Flamini, A.; Poli, N. *J. Chem. Soc., Dalton Trans.* **1993**, 2073−2074.
(66) Bonamico, M.; Fares, V.; Flamini, A.; Poli, N.; Mattei, G. *Polyhedron* **1993**, *12*, 1209−1214.
(67) Luger, P.; Buschmann, J. *Angew. Chem., Int. Ed. Engl.* **1983**, *22*, 410.
(68) Luo, X. L.; Schulte, G. K.; Crabtree, R. H. *Inorg. Chem.* **1990**, *29*, 682.
(69) Musselman, R. L.; Schneider, A. A. G. *Appl. Spectrosc.* **1987**, *41*, 106−110.
(70) Watkins, S. F. Morphang, Louisiana State University, Baton Rouge, LA 70803.

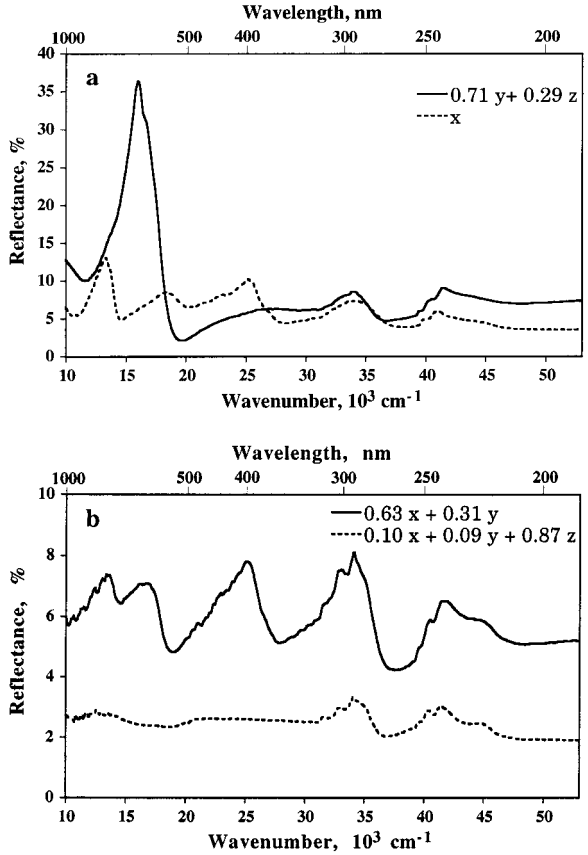

Figure 3. Polarized specular reflectance spectra of FeL_2·4THF: (a) off crystal face (00$\bar{1}$) with the electric vector parallel to the projected *x* (- - -) and perpendicular to the projected *x* (—); (b) off crystal face ($\bar{1}$10) with the electric vector parallel to the projected *z* (- - -) and perpendicular to the projected *z* (—).

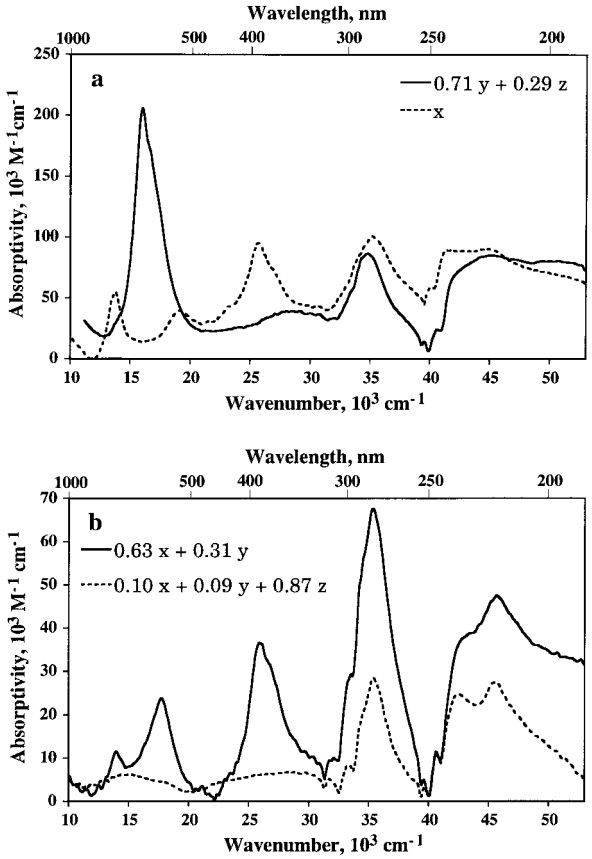

Figure 4. Polarized transformed absorbance spectra of FeL_2·4THF: (a) off crystal face (00$\bar{1}$) with the electric vector parallel to the projected *x* (- - -) and perpendicular to the projected *x* (—); (b) off crystal face ($\bar{1}$10) with the electric vector parallel to the projected *z* (- - -) and perpendicular to the projected *z* (—).

Table 3. Relative Contributions of Each Polarization to the Spectra

polarization	face	angle from elongated axis (deg)	I_x coeff	I_y coeff	I_z coeff
yz	(00$\bar{1}$)	+58.4	0.00	0.71	0.29
x	(001)	−31.6	1.00	0.00	0.00
xy	($\bar{1}$10)	+17.5	0.63	0.31	0.00
z	($\bar{1}$10)	−72.5	0.10	0.09	0.87

= the projected molecular vector component, and q = the angle between υ and the polarized light.

Spectroscopic Results. Reflectance spectra from the (00$\bar{1}$) and ($\bar{1}$10) faces are shown in Figure 3a,b. The results of Kramers−Kronig transformations are shown in Figure 4a,b. The enhancement in peak definition from the reflectance spectra is typical upon transformation into absorbance data. Figure 3a from the (00$\bar{1}$) face shows clear dichroism between the two polarizations, especially noticeable at 17 and 26 kcm^{-1}. This is consistent with our calculated molecular projections (100% *x* and 0% *x* for the two polarizations) on this face (see Table 3). While the energies of peaks are not dependent upon the choice of estimated reflectance beyond the experimental regions, the intensities are affected by those choices. In addition, the reflectance is affected by the surface quality of the natural crystal faces, which in turn affects the transformed absorbance. We have chosen estimated reflectances in the experimentally inaccessible regions so the transformed spectra match as closely as possible to the solution spectra, Figure 5. The energies of the transformed spectra clearly agree well with solution, especially at ~13, ~16, and 26 kcm^{-1}. To compare absorbance magnitudes, the transformed absorbances need to be adjusted

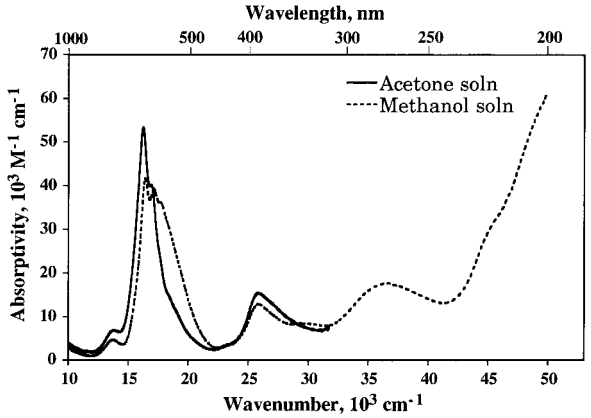

Figure 5. Solution spectra of FeL_2 in acetone (—) and methanol (- - -).

to solution-equivalent values (in solution, a polarization direction is aligned $^1/_3$ of the time with an electric vector; the polarized values thus need to be divided by 3). Since there may be some solid-state spectral effects,[43,45] we are not expecting exact agreement with solution. Upon this division, agreement with solution is reasonably good: the peak at 25.9 kcm^{-1} in Figure 4b (from the ($\bar{1}$10) face), for example, totals 14.2 × 10^3 M^{-1} cm^{-1} for both polarizations and the same peak in the solution spectrum in acetone is 15.4 × 10^3 M^{-1} cm^{-1}.

The individual polarizations were extracted using Gaussian deconvolution of the four polarized spectra off the (00$\bar{1}$) and ($\bar{1}$10) faces. First, of course, the pure *x*-polarized spectrum was Gaussian-deconvoluted in order to separate out the baseline;

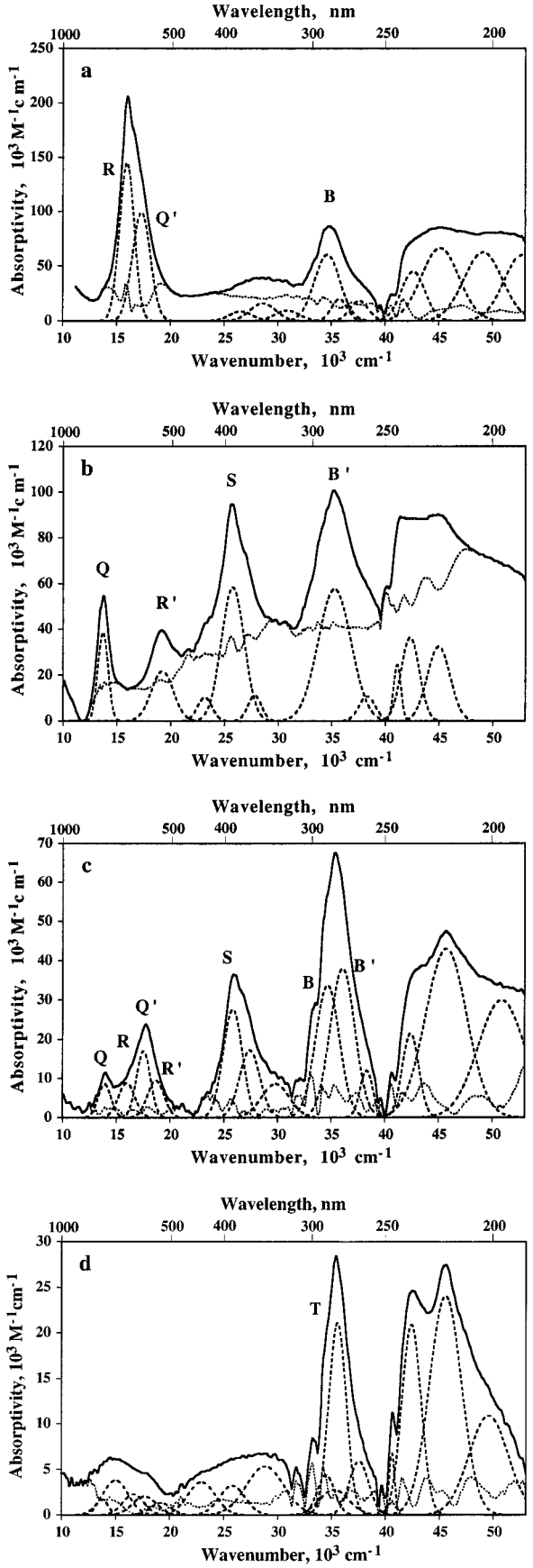

Figure 6. Deconvoluted spectra from FeL_2·4THF faces $(00\bar{1})$ and $(\bar{1}10)$. Polarizations: (a) *x*; (b) *yz*; (c) *xy*; (d) *z*. Key: experimental (—), Gaussian deconvolution (- - -); residual (···).

results are shown in Figure 6a. The peaks of principal interest are peaks Q, R′, S, and B′. Then, the energy and intensity values for these peaks were factored down according to Table 3 and entered into the deconvolution of the mixed *x*- and *y*-polarized spectrum from the $(\bar{1}10)$ face, Figure 6c. The remaining peaks were taken to be the *y*-polarized transitions. The appropriate intensities from the *x*- and *y*-polarized transitions were then used to extract the *z*-polarized transitions from the primarily *z*-polarized spectrum, Figure 6d. The mixed *y*- and *z*-polarized spectrum, Figure 6b, was used as a double-check on the *y* and *z* peaks, especially in the 35 kcm^{-1} region. Despite the inherent difficulty of obtaining accurate intensities via Kramers−Kronig transformation, the various absorption peaks showed remarkable consistency in the several spectra. We estimate the intensity reliability to be ±20%.

Discussion

The majority of electronic transitions in the porphyrins are allowed under electric vectors aligned in the *x* and *y* (in plane) directions. In D_{4h} symmetry the two directions are degenerate, and therefore, polarized studies of porphyrins provide only *x*,*y*-polarized and *z*-polarized transitions. D_{2h} systems, however, allow for separate *x* and *y* polarizations. In the present case of there having been different theoretical models proposed, the resultant assignments from these models in fact allow for a determination experimentally between the two. We will briefly review the theoretical models for porphyrins and a previous example of a metal phthalocyanine spectrum before illustrating the additional information obtainable from the present D_{2h} system. In addition, the presence of THF units arranged axially at the Fe center allow for additional transitions, including *z*-polarized transitions.

Theoretical Models. Gouterman's well-known four-orbital model of porphyrin rings[7,9,71] has been the standard for interpretation of porphyrin and related spectra. This model describes transitions between two HOMO levels, a_{2u} and a_{1u}, nearly degenerate in energy, and a pair of e_g LUMO orbitals. The nearly identical energies of the $a_{1u}{}^1e_g{}^1$ and $a_{2u}{}^1e_g{}^1$ states of the same symmetry (E_u) allow sufficient configuration interaction (CI) so that one combination of excited states, the B state, is ∼15 000 cm^{-1} above the other, the Q state. Experimentally, peak B is about 15 000 cm^{-1} above peak Q. In addition to the energy splitting consequence, the CI results in the lower energy transition's being forbidden. Thus the Q transition in porphyrins is predicted to be about $^1/_{10}$ the intensity of the Soret transition. In phthalocyanines (tetraazatetrabenzoporphyrins), the transition energies are similar for the Q region and the Soret region. The intensity of the Q transition, however, is about the same as the Soret transition. Gouterman explains this through Huckel calculations[25] which show a much greater energy difference between a_{1u} and a_{2u} in phthalocyanines than in porphyrins. This eliminates the CI and thus requires that the transitions be different in energy directly. It also removes the condition of forbiddenness, allowing Q to be as large as B. The coincidence required in this model is that CI in porphyrins results in exactly the same splitting as the transition energy difference without CI in the phthalocyanines.

An early alternate interpretation[72−74] for porphyrins and phthalocyanines was initiated about the same time: several transitions are predicted for the two main regions where Gouterman had predicted only one for each. A more recent

(71) Wang, M.-Y. R.; Hoffman, B. M. *J. Am. Chem. Soc.* **1984**, *106*, 4235.
(72) Henriksson, A.; Roos, B.; Sundbom, M. *Theor. Chim. Acta* **1972**, *27*, 303.
(73) Henriksson, A.; Sundbom, M. *Theor. Chim. Acta* **1972**, *27*, 213.
(74) Roos, B.; Sundbom, M. *J. Mol. Spectrosc.* **1970**, *36*, 8−25.

Table 4. Summary of Porphyrin Assignments Based on the Gouterman and Ellis Models[51]

peak	exptl energy (kcm^{-1})	Ellis orb trans	calcd energy (Ellis) (kcm^{-1})	Gouterman orb trans
Q	15.2	$2a_{1u}(\pi) \rightarrow 7e_g(\pi^*)$	13.1	$a_{1u}(\pi) \rightarrow e_g(\pi^*)$
R	18.0	$5a_{2u}(\pi) \rightarrow 7e_g(\pi^*)$	15.4	vib overtone of $a_{1u}(\pi) \rightarrow e_g(\pi^*)$
B	31.0	$6e_g(\pi) \rightarrow 4b_{2u}(\pi^*)$	32.3	$a_{2u}(\pi) \rightarrow e_g(\pi^*)$

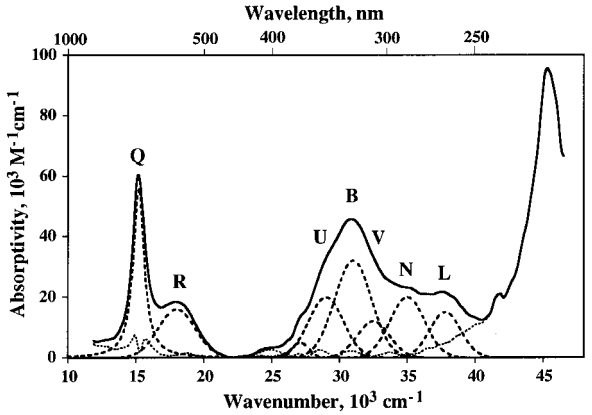

Figure 7. Deconvoluted in-plane absorbance spectrum of Cu(pc)I (from ref 51).

calculation comparing Ni(tbp) (tbp = tetrabenzoporphyrin) with Ni(pc)[46] has proven useful in comparing energies of MLCT and LMCT transitions in Co(pc)I and Ni(pc)I. Very recently, Ellis et al.[48] have used a density of states variation of the discrete variational X-α (DVXα-DOS) method to calculate transitions in pc's that agree especially well with experiment. Rende et al.[51] used them to interpret a series of M(pc)I's.

A spectrum and the interpreted results for Cu(pc)I are shown in Figure 7.[51] Assignments based upon the Gouterman and the Ellis models are summarized in Table 4. Gouterman et al. have assigned the Q and R peaks as being due to a single electronic transition: Q as the fundamental $a_{1u} \rightarrow e_g$ transition and R as its first vibrational overtone.[3,35,51,75] This is in contrast to the more recent interpretations made by this laboratory on the basis of calculations by Ellis et al.[48,51] in which the Q and R peaks are due to the separate transitions of $2a_{1u}(\pi) \rightarrow 7e_g(\pi^*)$ and $5a_{2u}(\pi) \rightarrow 7e_g(\pi^*)$. The B, or Soret, peak is assigned by Gouterman as $a_{2u}(\pi) \rightarrow e_g(\pi^*)$, the same as our assignment of peak R; we have assigned peak B as $6e_g(\pi) \rightarrow b_{2u}(\pi^*)$, with other transitions contributing slightly to the region.

It would be helpful to have a way to experimentally distinguish between the two sets of assignments. Fortunately, in the D_{2h} point group, we have found such a way. In D_{2h} symmetry, the degenerate D_{4h} e_g becomes b_{2g} and b_{3g}. The Q transition, $a_{1u} \rightarrow e_g$, is thus split into $a_u \rightarrow b_{3g}$ (*x* polarized) and $a_u \rightarrow b_{2g}$ (*y* polarized) components. Figure 8 summarizes the expected transitions under several conditions in the Q region from both the Gouterman and Ellis models. (The B region also results in splitting, but it is not as conclusive as the Q region.) Column **a** shows the assignment of D_{4h} transitions using both models. It is difficult to experimentally distinguish between them since both the Q and Q′ or R transitions are both allowed in the *x*,*y* directions. Columns **b** and **c** show two cases for D_{2h} related to the amount of e_g splitting: **b** shows the case of the splitting of e_g into b_{3g} and b_{2g} being less than the vibrational component (for the Gouterman model) or less than the a_u, b_{1u} energy difference (Ellis model). For the purposes of this comparison, we are assuming configuration interaction to be relatively small (as presumed by Gouterman for phthalocyanines) and thus are

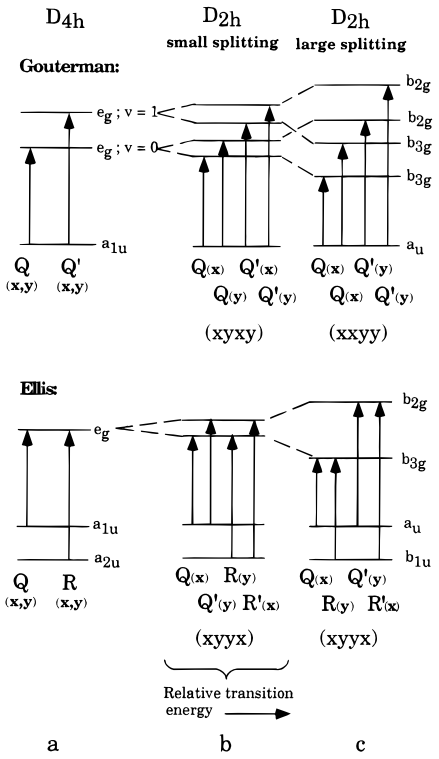

Figure 8. Transition diagrams for three cases each resulting from the Gouterman four-orbital model[7,9,71] and the Ellis Xα-DOS model[48] for metallophthalocyanine-type (Mpc) molecules: (a) D_{4h} Mpc with *x*,*y* degeneracy; (b, c) D_{2h} ML_2 with b_{2g}/b_{3g} smaller (b) or larger (c) than the symmetric vibrational component or the a_u/b_{1u} separation. The experimental energy order of *x* and *y* polarizations allows distinguishing between the two models.

estimating the transition energy to be equal to the difference in orbital energy levels. Column **c** shows the results with larger splitting which switches the order of the middle two transitions in both cases. If the ordering of the b_{2g} and b_{3g} orbitals is reversed, the *x* and *y* transitions would be switched in all cases. The transitions are listed in order of increasing energy to the right within each case. The expected ordering of transition polarizations in the Gouterman case **b** is *x*,*y*,*x*,*y* and in case **c** is *x*,*x*,*y*,*y* for the illustrated splitting order (b_{2g} being higher than b_{3g}). For either case the Ellis model predicts the ordering *x*,*y*,*y*,*x*.

Spectra. If one looks first at the Q region, 12−22 kcm^{-1}, in Figure 6a,b there are two *x*- and two *y*-polarized peaks. The *x*-polarized peaks in Figure 6a, Q and R′, are at 13.7 and 19.2 kcm^{-1}, and the *y*-polarized peaks in Figure 6b, R and Q′, are at 15.9 and 17.0 kcm^{-1}. Since the order is *x*,*y*,*y*,*x*, clearly this supports the Ellis model. We may therefore assign peak Q as $a_u \rightarrow b_{3g}$, peak R as $b_{1u} \rightarrow b_{3g}$, peak Q′ as $a_u \rightarrow b_{2g}$, and peak R′ as $b_{1u} \rightarrow b_{2g}$. The specific assignment of the two *y*-polarized transitions in the middle as R and Q′ is based on the shapes of the peaks: the R and R′ peaks are broader than Q and Q′. This assignment also results in the symmetry splitting's being the same for both pairs, 3.3 kcm^{-1}.

At higher energies, there are several prominent transitions: *x*-polarized peaks at 25.8 and 35.3 kcm^{-1}, an *xy* peak at ∼35 kcm^{-1}, and a *z* peak at 35 kcm^{-1}. Numerous smaller features appear to be present but we will focus on the principal peaks.

(75) Marks, T. J.; Stojakovic, D. R. *J. Am. Chem. Soc.* **1978**, *100*, 1695−1705.

Table 5. Experimental FeL_2·4THF Transitions

label	orb trans	energy (kcm^{-1})	area ($Å^2$)	polarization
Q	$a_u \rightarrow b_{3g}$	13.7	1.32	*x*
R	$b_{1u} \rightarrow b_{3g}$	15.9	6.2	*y*
Q′	$a_u \rightarrow b_{2g}$	17.3	4.7	*y*
R′	$b_{1u} \rightarrow b_{2g}$	19.2	1.15	*x*
S	$a_g(z^2) \rightarrow b_{3u}(p_x)$ or $b_{2g}(xz) \rightarrow b_{1u}(p_z)$	25.8	2.4	*x*
B	$b_{3g} \rightarrow b_{1u}$	34.6	2.1	*y*
B′	$b_{2g} \rightarrow b_{1u}$	35.2	2.5	*x*
T	$a_g(z^2) \rightarrow b_{1u}(p_z)$ or $b_{2g}(xz) \rightarrow b_{3u}(p_x)$	35.75	0.4	*z*

The nature of the *xy* peak at 35 kcm^{-1} needs some discussion. Both the *yz* and *xy* polarizations (Figure 4a,b) show peaks at 35 kcm^{-1}, and both the pure *x* and nearly pure *z* also show peaks at about 35 kcm^{-1}. The question that immediately arises is whether there is actually any *y* intensity at 35 kcm^{-1}. Upon a careful evaluation of Gaussian peaks in Figures 6a−d, we concluded that there is in fact a significant *y* absorption at 34.6 kcm^{-1} and a relatively small *z* absorption at 35.8 kcm^{-1} (see Table 5). Thus, there are *x*-, *y*-, and *z*-polarized transitions at ∼35 kcm^{-1}. In M(pc)I complexes, the Soret or B transition falls at about 32 kcm^{-1}, and in D_{2h}, the D_{4h} $e_g \rightarrow b_{2u}$ would split into $b_{2g} \rightarrow b_{1u}$ (*x* polarized) and $b_{3g} \rightarrow b_{1u}$ (*y* polarized) transitions; we propose that the *x* and *y* peaks at ∼35 kcm^{-1} are the Soret transitions. This provides for, of course, very little energy splitting due to lowered symmetry. We have carried out some preliminary ZINDO calculations of this system and find that the b_{2g}, b_{3g} split ranges from an average of 6 kcm^{-1} in the lowest 10 unoccupied orbitals to nearly zero for the highest occupied orbitals. Since we are proposing that the Soret peaks are due to transitions from occupied b_{2g} and b_{3g} orbitals, it is thus reasonable that we see little split in the energies of the Soret transitions.

In the 20−40 kcm^{-1} region, two prominent transitions remain unassigned: the *x*-polarized peak at 26 kcm^{-1} and the *z*-polarized peak at 35 kcm^{-1}. From arguments above, transitions related to planar complex orbitals should have both *x*- and *y*-paired components, and *z*-polarized transitions are not predicted by either Gouterman or Ellis for porphyrinic complexes. The transition at 26 kcm^{-1} is clearly not paired with a *y* transition. One major difference between this complex and the Mpc's or Mp's is the axial presence of two solvent molecules, THF's, with O's only 2.2 Å from the central Fe atom. Using σ_{sp} orbitals on the O's as a basis set, a_g and b_{1u} ligand group orbitals may be constructed which will combine with Fe d_{z^2} and p_z orbitals, respectively. As can be seen from Figure 1, the axial THF molecules are oriented normal to the complex's *x* axis. Using the π rings on THF as a basis set yields b_{3u} and b_{2g} orbitals which will combine with Fe p_x and d_{xz} orbitals, respectively. The most likely transitions involving these orbitals are shown in Table 5, transitions S and T. The immediate significance is that only *x*- and *z*-polarized transitions are involved. We are not yet able to determine which of the *x*-polarized transitions are responsible for the 26 kcm^{-1} peak and which of the *z*-polarized transitions are responsible for the 35 kcm^{-1} peak, but it seems reasonable to propose that those two peaks are due to one or two of each *x*- and *z*-polarized Fe−THF transitions, respectively.

The smaller surrounding peaks are reminiscent of the U and V peaks reported for the M(pc) complexes.[51] The region above 35 kcm^{-1} has yet to be interpreted. Calculations are not yet available for the entire region, and the numerous transitions will be better assigned upon their completion.

Conclusions

These spectra of FeL_2·4THF provide clear experimental evidence to allow support for a relatively new assignment of porphyrinic transitions. The transition assignments, summarized in Table 2, show the pattern *x*,*y*,*y*,*x* for the low-energy region. This ordering is not consistent with Gouterman's four-orbital model but is in agreement with Ellis's model based on X-α (DVXα) DOS calculations.

Acknowledgment. We thank the Progetto Finalizzato Materiali of Consiglio Nazionale delle Ricerche (CNR) for partial financial support. R.L.M. acknowledges the donors of the Petroleum Research Fund, administered by the American Chemical Society, Grant 25966-B3, the National Science Foundation Inorganic, Bioinorganic, and Organometallic Chemistry Program, Grant CHE-9521548, and the Hackman Scholars Program at Franklin and Marshall College (F&M) for financial support. The authors also thank Mr. Claudio Veroli of CNR for assistance in the X-ray structure determination and Mr. Davide Miksa of F&M for preliminary X-ray orientation work.

Supporting Information Available: A table providing a structure determination summary. This material is available free of charge via the Internet at http://pubs.acs.org.

IC980990D